Hydrol. Earth Syst. Sci. Discuss., 10, 11385–11422, 2013
www.hydrol-earth-syst-sci-discuss.net/10/11385/2013/
doi:10.5194/hessd-10-11385-2013

Hydrology and Earth System Sciences Discussions
Open Access

Imperfect scaling in distributions of radar-derived rainfall fields

M. J. van den Berg[1], **L. Delobbe**[2], **and N. E. C. Verhoest**[1]

[1]Laboratory of Hydrology and Water Management, Ghent University, Coupure links 653, 9000 Ghent, Belgium
[2]Royal Meteorological Institute, Avenue Circulaire 3, 1180 Uccle, Belgium

Received: 28 July 2013 – Accepted: 2 August 2013 – Published: 5 September 2013

Correspondence to: M. J. van den Berg (martinus.vandenberg@ugent.be)

Published by Copernicus Publications on behalf of the European Geosciences Union.

Abstract

Fine scale rainfall observations for modeling exercises are often not available, but rather coarser data derived from a variety of sources are used. Effectively using these data sources in models often requires the probability distribution of the data at the applicable scale. Although numerous models for scaling distributions exist, these are often based on theoretical developments, rather than on data. In this study, we develop a model based on the α-stable distribution of rainfall fields, and tested on 5 min radar data from a Belgian weather radar. We use these data to estimate functions that describe parameters of the distribution over various scales. Moreover, we study how the mean of the distribution and the intermittency change with scale, and validate and design functions to describe the shape parameter of the distribution. This information was combined into an effective model of the distribution. Finally, the model was fitted to data from numerous storms, and the resulting parameters were compared to investigate the change in scaling behavior through time.

1 Introduction

Hydrological models are used for a variety of applications such as watershed management (Rahman et al., 2009), flash flood predictions (Ferraris et al., 2002; Castelli, 1995; Rebora et al., 2006) and the hydrological projection of future climate models (Bergström et al., 2001; Dibike and Coulibaly, 2005). These models typically operate on a spatial scale of less than 100 km (Ferraris et al., 2003b) and a temporal scale of about an hour, thus requiring hydrological observations at a similar spatio-temporal scale. However, such data are often not available at the required scales.

Whenever suitable data are not available, the scaling behavior in rainfall can be exploited to yield an estimate of the rainfall at a finer scale. This can be done with a variety of methods, generally referred to as stochastic downscaling methods, which generally rely on the fractal, or scale invariant, behavior of rainfall. This behaviour of rainfall extends over a wide range of scales (Lovejoy and Schertzer, 1990, 2006; Lilley et al., 2006; Lovejoy et al., 2008, 2001) and is exploited to build various models to produce realistic rainfall fields in both space and time (Schertzer and Lovejoy, 1987; Gupta and Waymire, 1993; Menabde et al., 1997; Menabde and Sivapalan, 2000; Deidda, 2000; Koutsoyiannis et al., 2010; Lovejoy and Schertzer, 2010a). Although some more recent models use continuous cascades (Lovejoy and Schertzer, 2010a, b), most studies still use discrete cascades. This assumption of discreteness provides an attractive simplification of the equation, easing modelling and investigation, which gives some clue to their popularity. These discrete, multiplicative cascades pose that rainfall at spatial scale K can be modelled as

$$R_K = R_0 \prod_{k=0}^{K} W_k \,, \tag{1}$$

where R_K is a rainfall field at the scale to which the cascade is developed, and R_0 is the coarse departure field. In downscaling, R_0 is an observed rainfall field which is disaggregated, where each pixel is separately evolved according to the above equation. Hence Eq. (1) can be said to describe the evolution of a single pixel with decreasing size. Then, W_k is a multiplicative increment, which evolves the rainfall field from one scale to the next. Both $\ln(W_k)$ and $\ln(R_k)$ are assumed to be an α-stable random variable, with $\ln(W_k)$ assumed to be independent and identically distributed (iid) (Lovejoy and Mandelbrot, 1985). Hence, the actual value $\ln(W_k)$ is drawn from some α-stable distribution. Effectively, this creates volatility in the field at finer scales, where most pixels tend to have very small values, but a few have very large values. Then an observed rainfall field is effectively obtained by an integration of such a cascade, after it has been developed to infinitesimally fine scales, integrated to the resolution of interest. Such an integration is generally termed a dressed cascade, whereas the unintegrated version is referred to as the bare cascade (e.g. Deidda, 2000).

The above (simple) scaling model deals exclusively with the active rainfall pixels, i.e. those where it is raining. The reason for this is that rainfall is often assumed to be the result of two separate processes, and one for the support of the rainfall field which determines whether a pixel is wet or dry, and one for the actual rainfall intensity (Lovejoy and Mandelbrot, 1985). Several different models have been proposed for the support: those which assume a fractal support (e.g. Rebora et al., 2006), and those which assume that values below a certain threshold are zero (e.g. Ferraris et al., 2002). Evidently, the latter makes an assumption that is at odds with the earlier assumption that rainfall is the result of two distinct, but both fractal, processes and as a result this introduces a break in scaling behavior (Rupp et al., 2009). Nonetheless, practical analysis of this problem has proven difficult, and it remains unclear which assumption is the best.

Based on the above, a very basic downscaling model to develop the rainfall field is based on the use of Eq. (1) up to a scale $k = K$. Subsequently, the distinction between dry pixels and wet pixels is made using either the cut-off approach: $R_K \leq r_z = 0$, where r_z is some suitably chosen cut-off value; or, by developing a binary fractal field to the same resolution as the field and resetting R_K to $R_K \cdot I_K$, i.e. using the binary fractal field as a mask for the rainfall. Finally, the developed field, with dry pixels, is integrated back up to the scale of interest

$$R_{\text{target}}(i,j) = \frac{1}{l_k^2} \sum_{x=(i-1)l_k+1}^{il_k} \sum_{y=(j-1)l_k+1}^{jl_k} R_K(x,y)\,, \tag{2}$$

i.e. by taking the mean of the pixels within each of the coarser scale pixels at the scale of interest; l_k denotes the side length of the pixel at scale k in basic pixels, i.e. $l_k = 2^{K-k}$ where $K - k$ is used to reverse the scale.

To summarize the above, consider Fig. 1 where a simple downscaling model is described for a slice through a field. Figure 1a describes the bare cascade, where each rainfall value at a scale level k is multiplied with two values drawn from the distribution of W_k; in a 2-D setting, 4 values would be drawn. In contrast, Fig. 1b describes the dressing procedure, where each group of rainfall values at scale level $k-1$ is averaged to obtain the coarser scale pixel at scale level k.

HESSD
10, 11385–11422, 2013

Empirical investigation of the scaling behavior shows that not all rainfall fields obey the basic assumption that the increments between scales are iid. Divergences from this behavior were described by various authors who observed that the increments were dependent on factors such as large scale rainfall intensity (Deidda, 2000; Over and Gupta, 1994) and pixel size (Menabde et al., 1997; Over and Gupta, 1994; Paulson and Baxter, 2007). These deviations from perfect scaling are further examined in Veneziano et al. (2006); Serinaldi (2010), and Rupp et al. (2009), who showed that it is possible to model these imperfections in scaling through empirical functions of the parameters of various downscaling models.

The distributions involved in the above model are often assumed to belong to the family of α-stable distributions (Nolan, 2012), such that their logarithm is distributed as $\ln(R_k) \sim S_\alpha(-1, \gamma, \delta)$. The α-stable distribution S_α is said to be maximally skewed (Rupp et al., 2009), such that its positive moments do exist, or converge to a finite value, allowing for tractable analysis. Despite the obvious relationship between the downscaling model in Eq. (1) and these distributions, no suitable methods exist to reveal which distributions go with which cascades. Although no specific reason for this is known, this can be partly attributed to the fact that the moments in log-space do not uniquely relate to the moments in the untransformed space: $E[\log(R)^q] \leq E[\log(R)]^q$ for some moment q, evidently complicating the problem. Moreover, α-stable distributions have no closed form for their Cumulative Distribution Function (CDF) nor does it admit definitive forms of multivariate distributions, resulting in complicated analyses being required to obtain tractable results. Because of this, empirical models are used to relate the distributions to the downscaling model, e.g. see Rupp et al. (2009); Menabde et al. (1999).

In this paper, we wish to develop a model that directly estimates the distributions at various scales of the rainfall field. To do this, we have to approximate the distribution of $\ln(W)$, which may be dependent on scale. Moreover, there may be dependencies between the scale levels, which have to be taken into account. Hence, the following questions need to be investigated

HESSD
10, 11385–11422, 2013

- Is the distribution of $\ln(W_k)$ the same for all k?
- Is there dependence between the rainfall field $\ln(R_k)$ and its increment $\ln(W_k)$?
- Can we characterize the scaling behavior with a suitable set of equations such that it works for a large number of storms?

Additional to these question, it is interesting to know how well the model works for different rainfall fields. Moreover, characterizing the rainfall field as a set of functions allows us to gain some insight in the behavior of the distribution. As such, the following additional questions will be answered:

- Do the same functions provide an equal fit for all rainfall fields?
- How does the scaling behavior change through time?

This paper is structured as follows: in Sect. 2 the data are described, and transformations and operations on the data are explained and motivated. Section 3 presents a basic, preliminary, scaling analysis. In Sect. 4 the α-stable distribution and some of its basic properties are introduced, together with a suitable error measure. Then, the methodology is described in Sect. 5. Subsequently, the results are presented and discussed in Sect. 6. Finally, some conclusions and directions for future research are presented in Sect. 7.

2 Data

The data for this study were acquired by a C-band weather radar near Wideumont, Belgium, operated by the Belgian Royal Meteorological Institute (RMI). This installation covers a circular area with a radius of 240 km, producing a multi-level scan every five minutes. The region covered includes coastal landscapes to the west, and a low mountain range, the Ardennes, to the east with land cover mostly composed of forests,

HESSD
10, 11385–11422, 2013

urban development and agriculture. The entire region has a temperate climate and receives about 800 mm of rain annually, almost uniformly distributed throughout the year (De Jongh et al., 2006) and a mean monthly temperature which varies between 18 °C in June and 3 °C in January.

The actual 5 min radar images are taken from large events during 2009, with 9 winter storms and 17 summer storms. These images were extracted from a 6 month time series during which larger storm episodes were selected to ensure sufficient data. These images correspond to the basic 5 min interval images, however, to reduce the data load, we opted to use only the first image of each hour. The images used were not aggregated in order to retain the basic spatial scaling behavior as well as to avoid ripple effects (Delobbe et al., 2006) and possible temporal scaling.

The raw radar data are produced by a 5-elevation scan performed every 5 min. Measurements are collected up to 240 km with a resolution of 250 m in range and 1° in azimuth. A time-domain Doppler filtering is applied for ground clutter removal. An additional treatment, based on a static clutter map, is applied to eliminate residual permanent ground clutter (e.g. buildings). The radar data are then stored as digital numbers representing the reflectivity values ranging from −31.5 dB to 95.5 dB in steps of 0.5 dB. A two-dimensional radar product is then extracted from the three-dimensional polar data on a Cartesian grid with a resolution of 0.6 km × 0.6 km (Goudenhoofdt and Delobbe, 2009). Reflectivity values are then converted into precipitation rates using

$$R_0 = \sqrt[b]{\frac{10^{0.1 \cdot Z_{\mathrm{dB}}}}{a}}, \tag{3}$$

where Z_{dB} is the reflectivity in [dB] and a and b are dimensionless parameters, respectively equal to 200 and 1.6. Finally, only the inner 100 km are used in the analysis, as the radar does not produce reliable quantitative estimates outside this range. A sample data image is shown in Fig. 2, where the black circle denotes the 100 km range. Small deviations from this circle are allowed to accommodate the square, aggregated pixels. Additionally, if the image contains less than 10 % active pixels, the image is discarded.

HESSD
10, 11385–11422, 2013

Title Page
Abstract Introduction
Conclusions References
Tables Figures
◀◀ ▶▶
◀ ▶
Back Close
Full Screen / Esc
Printer-friendly Version
Interactive Discussion

The processed data were artificially downgraded to obtain a scale cascade of each rainfall image with scales ranging from a pixel size of 0.6 km × 0.6 km to 9.6 km × 9.6 km, with factors $l_k = 2^{K-k} \cdot 0.6$ km where $k = 0...4$. These degraded pixels are obtained by spatially averaging the rainfall depths over squares of the appropriate size (Ferraris et al., 2003a; Deidda, 2000). Thus, the relation between the fine scale field R_k and the coarse scale field R_0, can be expressed through Eq. (2). Generally, the scale of the pixels is expressed as

$$\lambda_k = \frac{l_k}{L_{\text{eff}}}, \tag{4}$$

where L_{eff} is the effective outer scale at which the moments converge. This is an a-priori unknown quantity, which has to be estimated from the data (Lovejoy et al., 2008).

3 Scaling analysis

A first step in the analysis of scaling behavior is to establish whether or not the rainfall field is actually scaling, and whether this scaling is multifractal. To provide some insight into this, a single image was analyzed, shown in Fig. 2. For this analysis the field was made conservative by transforming it as (Lovejoy et al., 2008)

$$R_{\lambda_K}^{\text{cons}} = \frac{|\nabla^2(R_{\lambda_K})|}{\langle|\nabla^2(R_{\lambda_K})|\rangle}, \tag{5}$$

where ∇^2 is the 2-D laplacian, and $\langle\cdot\rangle$ denotes the average of the field.

A first tool to assess the scaling behavior is the radially averaged power spectrum, shown in Fig. 3. This figure analyses the full image, without any cutoffs or modifications. In this image, the expectation is to find a linear slope, indicating scaling behavior. Such behavior is observed, as indicated by the linear fit, although a small deviation exists

HESSD
10, 11385–11422, 2013

at lower scales. This break is likely due to the threshold of the rainfall field as a result of the radar not being able to accurately measure rainfall intensities below 0.1 mm h^{-1} (Lovejoy et al., 2008).

A basic principle of multifractal behavior is that the (empirical) moments scale as

$$\frac{\langle R_k^q \rangle}{\langle R_0^q \rangle} = \left(\frac{l_k}{L_{\mathrm{ref}}} \right)^{K(q)}, \tag{6}$$

where R_k is the rainfall field at scale $l = 2^{(K-k)} \cdot 0.6$. L_{ref} is a conveniently chosen outer scale, in lieu of knowing the effective outer scale, and $K(q)$ is the moment scaling function. This function illustrates that if the field is multifractal, the various empirical estimates of a moment q should lie on a straight line in a log-log plot of $\langle R_k^q \rangle / \langle R_0^q \rangle$ against the scale λ_k. By plotting these lines for a variety of moments, shown in Fig. 4, the linearity, and thus multifractal scaling behavior, of each moment can be assessed. As can be seen, these lines are close to linear, further suggesting fractal behavior. The outer scale is the point at which all lines intersect (Lovejoy et al., 2008). This analysis is shown in Fig. 4, for the conservative field, and all moments appear to be appropriately scaling (i.e. linear), which is further confirmed by a Double Trace Moment analysis (Veneziano et al., 2006) shown in Fig. 5. The intersection point L_{eff} can be difficult to find, as small deviations from linear behavior may prevent the lines from converging. This is solved by forcing the regression lines to convergence at a point for which the RMSE is minimal. Based on this, the effective outer scale for this particular image was found to be about 643 km for this particular storm. However, we should note that such an analysis can be inaccurate, and should only be used as a reference.

4 α-stable distributions

As mentioned in the introduction, the logarithm of the rainfall fields R_k and their increments W_k are assumed to be distributed according to the α-stable distribution. The

HESSD
10, 11385–11422, 2013

α-stable family of distributions allows for a large variety in behavior, including right- and left-skewed behavior, as well as symmetric behavior. Furthermore, the distribution allows either a heavy tail or a light, vanishing, tail on either side, or on both sides, of the mode. Due to this highly flexible behavior, it includes several well-known distributions such as the Normal distribution and the Cauchy distribution. The α-stable distribution does not have a closed form, but rather expresses its density as an integral of the characteristic (moment-generating) function over all moments ranging from $-\infty$ to $+\infty$. This would result in an indefinite integral that only has a closed form in a few special cases. Hence, an approximation is required. Although various different approximations exist, they are all roughly equivalent and here we used that of Nolan (1997), as implemented in the R-package *stabledist* Wuertz et al. (2012).

There are a number of different parametrizations available for the α-stable distribution, all suitable for different purposes; we opted for the S1 parametrization of Nolan (2012). Given this parametrization, different α-stable distributions with (necessarily) the same stability parameter α^{s}, which mainly determines the heaviness of the tail, can be summed as

$$\alpha_Z^{\mathrm{s}} = \alpha_X^{\mathrm{s}} = \alpha_Y^{\mathrm{s}} = \alpha^{\mathrm{s}}, \tag{7}$$

$$\beta_Z = \frac{\beta_X \gamma_X^{\alpha^{\mathrm{s}}} + \beta_Y \gamma_Y^{\alpha^{\mathrm{s}}}}{\gamma_X^{\alpha^{\mathrm{s}}} + \gamma_Y^{\alpha^{\mathrm{s}}}}, \tag{8}$$

$$\gamma_Z^{\alpha^{\mathrm{s}}} = \gamma_X^{\alpha^{\mathrm{s}}} + \gamma_Y^{\alpha^{\mathrm{s}}}, \tag{9}$$

$$\delta_Z = \delta_X + \delta_Y. \tag{10}$$

Here $\alpha^{\mathrm{s}} \in (0,2]$ is a stability parameter, or volatility index, which is necessarily the same for all distributions involved in the above summation. The parameter β represents the skewness and ranges from -1 to 1, where 0 represents symmetry, $\gamma > 0$ is the shape parameter and the shift parameter $-\infty \leq \delta \leq \infty$ controls the location of the distribution.

When $\alpha^{\mathrm{s}} = 2$, the α-stable distribution becomes the normal distribution. As a result, the effect of the parameter β diminishes as $\alpha^{\mathrm{s}} \to 2$ and has no effect when $\alpha^{\mathrm{s}} = 2$ as

HESSD
10, 11385–11422, 2013
Imperfect scaling in rainfall
van den Berg et al.

the normal distribution is necessarily symmetric. Additionally, when $\alpha^s = 2$, the shift parameter δ is equal to the mean, and the shape parameter relates to the variance as $\sigma^2 = \sqrt{\gamma}/2$. Additionally, the distribution only has moments that are smaller than α^s, hence, if $\alpha^s \geq 1$ the shift parameter is equal to the mean. Moreover, when $\beta = -1$, the distribution is entirely left-skewed, meaning that it only has a "fat" tail towards the left. Consequentially, the positive moments converge, whereas the negative moments do not. Fortunately, as we generally only deal with positive moments in rainfall analysis, this property allows for an easy analysis.

The α-stable distribution can be fitted in a variety of ways, including the well-known Maximum Likelihood method. Nevertheless, fitting α-stable distributions is still a difficult exercise, partly due to the lack of a closed form. Despite these difficulties, numerous different approaches are available and a summary of these approaches can be found in Nolan (1999). For this study, the method of Koutrouvelis (1980) is used together with that of McCulloch (1986). Although an in depth explanation is not within the scope of this paper, the method of McCulloch (1986) relies on a look up table of quantile values and associated parameter values, which is interpolated to obtain a crude first guess estimate of the parameters for the second step. The second step, that of Koutrouvelis (1980), relies on an iterative regression on the characteristic function, together with its empirical counterpart. Essentially, the parameters are updated stepwise by regressing them against the empirical characteristic function $E[\exp(\sqrt{-1}qX)]$ for moment q.

Although the above methods produce accurate results in a fast and convenient manner, it was observed that the actual results tend to be biased, often as a result of truncated tails in the data. This was mitigated by two procedures. First, several parameters were fixed a priori, namely $\beta = -1$ and $\delta = E[X]$ where the latter obviously relies on $\alpha \geq 1$. Evidently, fixing $\beta = -1$ ensures that the positive moments converge, and the second assumption $\delta = E[X]$ ensures that the averages between the fitted and the empirical probability distributions match. Moreover, the resulting fits were further optimized using a local simplex search to find the optimal parameter set. The resultant parameters provided a better fit than the raw output from the basic fitting algorithm.

HESSD
10, 11385–11422, 2013

Finally, to quantify the quality of the fit, the Earth Movers Distance (EMD) is used. The EMD is a measure similar to other error measures such as the Root Mean Squared Error and the Mean Absolute Error (van den Berg et al., 2011; Rubner and Tomasi, 1999), however, it accounts for both vertical and horizontal differences between probability distribution functions such that, for example, shifts in mean are appropriately taken into account. This difference between RMSE and EMD becomes important when the distribution has a strong peak, such as exponential-like distributions. As these can be encountered in the subset of the α-stable distribution, this metric shows a more stable performance than does the RMSE.

5 Methodology

The starting point for any analysis is the rainfall intensity field R_0. In this study, the resolution of these images is degraded to find a synthetic cascade, using Eq. (2). The result is a set of rainfall images R_k with $k \in (0..K)$ with increasing (coarsening) scale. By taking the log-transform of these fields, the log-increments $\ln(W_k), k \in (0..K-1)$ can be extracted as

$$\ln(W_k) = \ln(R_{k+1}) - \ln(R_{k+1}) = \ln\left(\frac{R_k}{R_{k+1}}\right), \tag{11}$$

where the difference in the number of pixels is overcome by repeating the action for each pixel and its coarse scale pixel. The resulting cascades can then be analyzed by fitting an α-stable distribution to each of the fields $\ln(W_k)$ and $\ln(R_k)$ for $k \in (0..K)$. Moreover, as mentioned earlier, the parameter α^{s} should be the same for all these distributions. Therefore, the fit is done in two steps, first a preliminary step where all distributions are fitted separately resulting in a set $\alpha^{\mathrm{s}}_{i=0..K}$, which contains all values α^{s} for both the increments and the fields. Then, the distributions are fitted a second time, forcing $\alpha^{\mathrm{s}} = \langle\alpha^{\mathrm{s}}_{i=0..K}\rangle$. Although no formal relationship exists between distributions with different α^{s}, it was found that the mean of a set was in good agreement with optimized

HESSD
10, 11385–11422, 2013

values of α^s. Hence, this analysis results in a set of parameters $(\alpha^s_W, -1, \gamma_{W_k}, \delta_{W_k})$ for each scale level k, where it should be noted that δ_{W_k} is forced to be equal to $\langle \ln(W_k) \rangle$. A similar set is found for each rainfall field $\ln(R_k)$, denoted by subscript R_k.

Besides the basic parameters of the distribution, we are also interested in establishing whether or not the fields and their increments are actually iid. A simple test would be to use the correlation to assess whether or not these distributions are uncorrelated. However, the α-stable distribution with stability parameter α^s does not admit moments $q > \alpha^s$, hence, if $\alpha^s < 2$ the (Pearson) correlation does not exist. As a result, using raw correlations is not feasible, and a difficult problem in α-stable analysis arises. Many different measures have been suggested, but to the authors' knowledge all of these pertain to symmetric distributions, i.e. those with $\beta = 0$. Nonetheless, we adopt the correlation value of Garel and Kodia (2009) as it offers important benefits and presents a conceptually simple framework.

The basis of the correlation value of Garel and Kodia (2009) relies on the notion that, for properly scaled variables with finite second order moments, the slope of the regression $E[R|W] = E[W|R]$ (note that the logarithm and the scale indicators have been dropped for notational convenience) is equal to the Pearson correlation ρ. However, the regression line and its slope always exist, in contrast to the Pearson correlation coefficient, even though we cannot generally say that it is finite or exchangeable (i.e. it could be that $E[R|W] \neq E[W|R]$). Hence, an appealing correlation measure is

$$\varrho(R, W) = \operatorname{sign}(\theta_{R|W}) \sqrt{\theta_{R|W} \theta_{W|R}}, \tag{12}$$

where $\theta_{R|W}$ is the slope of the regression line $E[R|W]$, and similarly for $\theta_{W|R}$. Use of the square root is to ensure that if the second order moment exists, the metric coincides with the Pearson correlation. Finally, the sign function is used to ensure that negative and positive correlations are differentiated. A proof for this metric is beyond scope of the paper, rather, we will investigate its practical skill.

The relationship between the shape parameters of the rainfall field and its increments, γ_W and γ_R, with $\varrho(R, W) \neq 0$ is dependent on the entire bivariate distribution

(Nolan, 2012). However, modeling such a distribution is highly cumbersome and not at all evident as multivariate stable distributions are an area of ongoing research; Therefore, a simplification is needed. We observe that if $\alpha^{s} = 2$ the relationship between γ_W and γ_R is

$$\gamma_{R+W}^{\alpha^{s}} = \gamma_R^{\alpha^{s}} + \gamma_W^{\alpha_S} + \rho(2\sigma_R^{\alpha^{s}})^{(1/\alpha^{s})}(2\sigma_W^{\alpha^{s}})^{(1/\alpha^{s})}, \tag{13}$$

where ρ denotes the Pearson correlation coefficient. The above is dependent on the notion that if $\alpha^{s} = 2$ the α-stable distribution becomes a normal distribution, with variance $2\gamma^{\alpha^{s}}$. Therefore, to simulate the effects of the summation of a correlated distribution, we use Eq. (13) where we substitute ρ with ϱ. The effects of using this equation are investigated in Fig. 6 by comparing shape parameters fitted to the empirical distribution with shape parameters computed according to Eq. (13). Note that, in general, the errors appear to be mild, however, at lower values of α^{s}, several large errors can be observed. Fortunately, few rainfall images have distributions with low α^{s}, making this a tenable assumption.

To investigate the behavior of the scaling of the α-stable parameters through time, we first need to characterize this behavior for each of the images. This is done by fitting a set of scale dependent functions to the α-stable parameters for each image and its increments. The mean behavior of the α-stable parameters for all images was used as a guideline for the function forms, shown in Figs. 7 to 9. These empirical functions all admit relatively simple function forms, namely

$$\delta_k = a_\delta + b_\delta \cdot \ln(\lambda), \tag{14}$$

$$\gamma_k = e^{a_\gamma + b_\gamma \cdot \ln(\lambda)}, \tag{15}$$

$$\varrho_k = a_\varrho + b_\varrho \cdot \frac{1}{\lambda}. \tag{16}$$

Note that the subscripts identifying that these parameters apply to $\ln(W_k)$ have been dropped for notational convenience. The exponent in the function for γ_k ensures that the range is $[0, \infty[$. The equation for ϱ is not bounded as the correlation measure used is not. The fit of the above functions is examined in Figs. 7 to 9, for each of the parameters respectively. The confidence intervals of each of the functions are relatively small, and the behavior is well respected. Nevertheless, the function for δ_k appears to have a slight curve to it, possibly suggesting a more complex behavior. However, due to the limited number of scale levels available fitting a more complex function was not feasible.

To summarize the above, we retake Fig. 1, specifically the distribution $W_0 \sim S_\alpha(-1, \gamma_0, \mu_0)$ and the same distribution at further scales. The values γ_k and δ_k at all scales are found through Eqs. (14) to (16). Then, having the distribution of the coarsest scale rainfall, $\ln(R_0)$, we can find R_1 using ϱ_0 applying Eq. (13) with ρ substituted with ϱ. Applying this framework iteratively, it is possible to find R_2 and so on.

Finally, the number of dry pixels are modeled based on the fractal box counting dimension (Rupp et al., 2009). As the boxcounting dimension is directly based on the number of dry pixels at each scale, it suffices to invert this relationship

$$P(Y > 0)_l = \left(\frac{1}{l_k}\right)^{D_\mathrm{f}} \cdot P(Y > 0)_{l_k = 1} \tag{17}$$

where D_f is the fractal dimension and l_k is the side length of the pixel at scale k expressed in elementary pixels. This relationship performs near perfect (Fig. 10).

6 Scaling behavior

In Fig. 11 all the correlations for each of the scales are shown, summarized as a boxplot. From this plot, it is evident that almost all storms exhibit a negative correlation between the increments and the rainfall field. This pattern is also seen in rank correlation measures (not shown), further corroborating that there is indeed negative correlation. Taking this negative correlation into account according to Eq. (13) indeed results in a decrease in error, as is evidenced by the lower EMD for the correlated than for the

HESSD
10, 11385–11422, 2013

uncorrelated error (Fig. 12). Moreover, the significant decrease in the shape parameter, γ further suggest that the iid assumption is, for these storms, incorrect.

The functions (14) to (16) are used to characterize the scaling behavior. These functions exhibit a good fit for all storms, as determined through the relative error (Fig. 13). The resulting parameters are shown for each storm in Figs. 14 to 16. From these boxplots, it can be seen that summer storms exhibit a higher spread of all parameter values and a higher mean of the increments. However, the ϱ shows no difference in intercept, but the decrease in ϱ for winter storms is higher than for summer storms. However, there is no real clear pattern distinguishing the behavior between the winter and summer storms.

The analyses confirm the common finding summer that storms tend to be more energetic with higher variances and higher mean rainfall. Moreover, summer storms appear to exhibit a smaller decrease in correlations, resulting in a stronger correlation at the lower scale levels.

Figure 17 shows the difference between the EMDs of the modeled distributions and the direct fitted distributions, propagated over the four scale levels. It can be seen that the model increases the EMD as the number of scale levels increases. Nonetheless, the error remains relatively low, showing that the model captures the scaling behavior quite well. The fractal model for the dry pixels works very well, as should be expected due to the direct relation with the actual number of dry pixels.

7 Conclusions

In this paper, we investigated the scaling behavior of the distributions of rainfall. To this end, a novel scaling model was introduced that only relies on the basic assumptions regarding the cascade structure responsible for the fractal nature of rainfall. Furthermore, this framework is based on direct empirical comparison with the observed distributions. In contrast, most previous work relied on theoretical considerations and indirect use of the scaling distributions. Therefore, this framework allows for a more direct and empirical investigation into the scaling behavior of rainfall, and provides a more adaptable framework to be used for practical purposes.

The empirical investigation into the distribution showed that the shape parameter, loosely related to the variance, of finer scales is smaller than its parent scale. This contradicts the classical scaling theory (Lovejoy and Mandelbrot, 1985) that uncorrelated increment distributions are added, as this would cause an increase in the shape parameter. Moreover, it was shown that it is possible to improve these predictions by taking into account the correlation. Although the method used to add the correlations is only correct when $\alpha^s = 2$, using an approximate equation improved performance. This suggests that there is, in fact, imperfect scaling in all of the investigated images.

In this paper, imperfect scaling behavior was characterized using three simple equations (Eqs. 14 to 16). It was found that these equations fit well, and are successful in describing the general behavior of the distribution for all observed images.

In future research, the full dependence structure will need to be evaluated to allow for a more accurate representation of the dependence between scale levels and their increments. This will allow for a deeper investigation into this aspect of imperfect scaling and possible a better way of representing the scaling behavior. Finally, the difference with respect to the scaling behavior, between convective and stratiform storms will need further investigation, using a classification algorithm such as the Steiner algorithm (Steiner et al., 1995). A careful analysis of the behavior of such algorithms will be required before using them to investigate the difference in scaling behaviour between stratiform and convective precipitation.

Acknowledgements. We wish to thank the Special Research Fund (B.O.F.) of Ghent University and the Flanders Research Fund (FWO, Grant Number: G.0837.10) for funding this research.

References

Bergström, S., Carlsson, B., Gardelin, M., Lindstrom, G., Pettersson, A., and Rummukainen, M.: Climate change impacts on runoff in Sweden – assessments by global climate models, dynamical downscaling and hydrological modelling, Clim. Res., 16, 101–112, 2001. 11386

Castelli, F.: Atmosphere modeling and hydrologic-prediction uncertainty, invited lecture at the US-Italy Workshop on the Hydrometeorology, Impacts and Management of Extreme Floods, Perugia, Abstract 2.2, 13–17 November, 1995. 11386

De Jongh, I. L. M., Verhoest, N. E. C., and De Troch, F. P.: Analysis of a 105-year time series of precipitation observed at Uccle, Belgium, Int. J. Climatol., 26, 2023–2039, 2006. 11391

Deidda, R.: Rainfall downscaling in a space-time multifractal framework, Water Resour. Res., 36, 1779–1794, 2000. 11387, 11389, 11392

Delobbe, L., Dehem, D., Dierickx, P., Roulin, E., Thunus, M., and Tricot, C.: Combined use of radar and gauge observations for hydrological applications in the Walloon region of Belgium, in: Proceedings of ERAD, Barcelona, 418–421, 2006. 11391

Dibike, Y. B. and Coulibaly, P.: Hydrologic impact of climate change in the Saguenay watershed: comparison of downscaling methods and hydrologic models, J. Hydrol., 307, 145–163, 2005. 11386

Ferraris, L., Rudari, R., and Siccardi, F.: The uncertainty in the prediction of flash floods in the northern Mediterranean environment, J. Hydrometeorol., 3, 714–727, 2002. 11386, 11388

Ferraris, L., Gabellani, S., Parodi, U., Rebora, N., Von Hardenberg, J., and Provenzale, A.: Revisiting multifractality in rainfall fields, J. Hydrometeorol., 4, 544–551, 2003a. 11392

Ferraris, L., Gabellani, S., Rebora, N., and Provenzale, A.: A comparison of stochastic models for spatial rainfall downscaling, Water Resour. Res., 39, 1368, doi:10.1029/2003WR002504, 2003b. 11386

Garel, B. and Kodia, B.: Signed symmetric covariation coefficient for alpha-stable dependence modeling, CR Math., 347, 315–320, 2009. 11397

Goudenhoofdt, E. and Delobbe, L.: Evaluation of radar-gauge merging methods for quantitative precipitation estimates, Hydrol. Earth Syst. Sci., 13, 195–203, doi:10.5194/hess-13-195-2009, 2009. 11391

Gupta, V. K. and Waymire, E. C.: A statistical analysis of mesoscale rainfall as a random cascade, J. Appl. Meteorol., 32, 251–251, 1993. 11387

Koutrouvelis, I.: Regression-type estimation of the parameters of stable laws, J. Am. Stat. Assoc., 75, 918–928, 1980. 11395
Koutsoyiannis, D., Paschalis, A., and Theodoratos, N.: Two-dimensional Hurst–Kolmogorov process and its application to rainfall fields, J. Hydrol., 398, 91–100, 2010. 11387
Lilley, M., Lovejoy, S., Desaulniers-Soucy, N., and Schertzer, D.: Multifractal large number of drops limit in rain, J. Hydrol., 328, 20–37, 2006. 11387
Lovejoy, S. and Mandelbrot, B. B.: Fractal properties of rain, and a fractal model, Tellus A, 37, 209–232, 1985. 11387, 11388, 11401
Lovejoy, S. and Schertzer, D.: Fractals, raindrops and resolution dependence of rain measurements, J. Appl. Meteorol., 29, 1167–1170, 1990. 11387
Lovejoy, S. and Schertzer, D.: Multifractals, cloud radiances and rain, J. Hydrol., 322, 59–88, 2006. 11387
Lovejoy, S. and Schertzer, D.: On the simulation of continuous in scale universal multifractals, Part I: Spatially continuous processes, Comput. Geosci., 36, 1393–1403, 2010a. 11387
Lovejoy, S. and Schertzer, D.: On the simulation of continuous in scale universal multifractals, Part II: Space-time processes and finite size corrections, Comput. Geosci., 36, 1404–1413, 2010b. 11387
Lovejoy, S., Schertzer, D., and Stanway, J. D.: Direct evidence of multifractal atmospheric cascades from planetary scales down to 1 km, Phys. Rev. Lett., 86, 5200–5203, 2001. 11387
Lovejoy, S., Schertzer, D., and Allaire, V. C.: The remarkable wide range spatial scaling of TRMM precipitation, Atmos. Res., 90, 10–32, 2008. 11387, 11392, 11393
McCulloch, J.: Simple consistent estimators of stable distribution parameters, Commun. Stat. Simulat., 15, 1109–1136, 1986. 11395
Menabde, M. and Sivapalan, M.: Modeling of rainfall time series and extremes using bounded random cascades and Levy-stable distributions, Water Resour. Res., 36, 3293–3300, 2000. 11387
Menabde, M., Harris, D., Seed, A., Austin, G., and Stow, D.: Multiscaling properties of rainfall and bounded random cascades, Water Resour. Res., 33, 2823–2830, 1997. 11387, 11389
Menabde, M., Seed, A., and Pegram, G.: A simple scaling model for extreme rainfall, Water Resour. Res., 35, 335–339, 1999. 11389
Nolan, J. P.: Parameter estimation and data analysis for stable distributions, in: Conference Record of the Thirty-First Asilomar Conference on Signals, Systems & Computers, 1997, vol. 1, IEEE, Pacific Grove(CA), USA, 443–447, 1997. 11394

Nolan, J. P.: Fitting data and assessing goodness-of-fit with stable distributions, unpublished manuscript, American University, Washington, DC, 1999. 11395
Nolan, J. P.: Stable Distributions – Models for Heavy Tailed Data, Birkhauser, Boston, in progress, Chapter 1 available at: http://academic2.american.edu/~jpnolan (last access: 20 August 2013), 2012. 11389, 11394, 11398
Over, T. and Gupta, V.: Statistical analysis of mesoscale rainfall: dependence of a random cascade generator on large-scale forcing, J. Appl. Meteorol., 33, 1526–1542, 1994. 11389
Paulson, K. S. and Baxter, P. D.: Downscaling of rain gauge time series by multiplicative beta cascade, J. Geophys. Res., 112, D09105, doi:10.1029/2006JD007333, 2007. 11389
Rahman, S., Bagtzoglou, A. C., Hossain, F., Tang, L., Yarbrough, L. D., and Easson, G.: Investigating spatial downscaling of satellite rainfall data for streamflow simulation in a medium-sized basin, J. Hydrometeorol., 10, 1063–1079, 2009. 11386
Rebora, N., Ferraris, L., von Hardenberg, J., and Provenzale, A.: Rainfall downscaling and flood forecasting: a case study in the Mediterranean area, Nat. Hazards Earth Syst. Sci., 6, 611–619, doi:10.5194/nhess-6-611-2006, 2006. 11386, 11388
Rubner, Y. and Tomasi, C.: Texture-based image retrieval without segmentation, in: The Proceedings of the Seventh IEEE International Conference on Computer Vision, 1999, vol. 2, IEEE, Corfu, Greece, 1018–1024, 1999. 11396
Rupp, D. E., Keim, R. F., Ossiander, M., Brugnach, M., and Selker, J. S.: Time scale and intensity dependency in multiplicative cascades for temporal rainfall disaggregation, Water Resour. Res., 45, W07409, doi:10.1029/2008WR007321, 2009. 11388, 11389, 11399
Schertzer, D. and Lovejoy, S.: Physical modeling and analysis of rain and clouds by anisotropic scaling multiplicative processes, J. Geophys. Res., 92, 9693–9714, 1987. 11387
Serinaldi, F.: Multifractality, imperfect scaling and hydrological properties of rainfall time series simulated by continuous universal multifractal and discrete random cascade models, Nonlinear Proc. Geoph., 17, 697–714, 2010. 11389
Steiner, M., Houze Jr., R. A., and Yuter, S. E.: Climatological characterization of three-dimensional storm structure from operational radar and rain gauge data, J. Appl. Meteorol., 34, 1978–2007, 1995. 11401
van den Berg, M. J., Vandenberghe, S., De Baets, B., and Verhoest, N. E. C.: Copula-based downscaling of spatial rainfall: a proof of concept, Hydrol. Earth Syst. Sci., 15, 1445–1457, doi:10.5194/hess-15-1445-2011, 2011. 11396

HESSD
10, 11385–11422, 2013

Title Page
Abstract | Introduction
Conclusions | References
Tables | Figures
◀| |▶
◀ ▶
Back | Close
Full Screen / Esc
Printer-friendly Version
Interactive Discussion

Veneziano, D., Furcolo, P., and Iacobellis, V.: Imperfect scaling of time and space-time rainfall, J. Hydrol., 322, 105–119, 2006. 11389, 11393
Wuertz, D., Maechler, M., and R core team members: stabledist: Stable Distribution Functions, r package version 0.6-5, available at: http://CRAN.R-project.org/package=stabledist, 2012. 11394

HESSD
10, 11385–11422, 2013

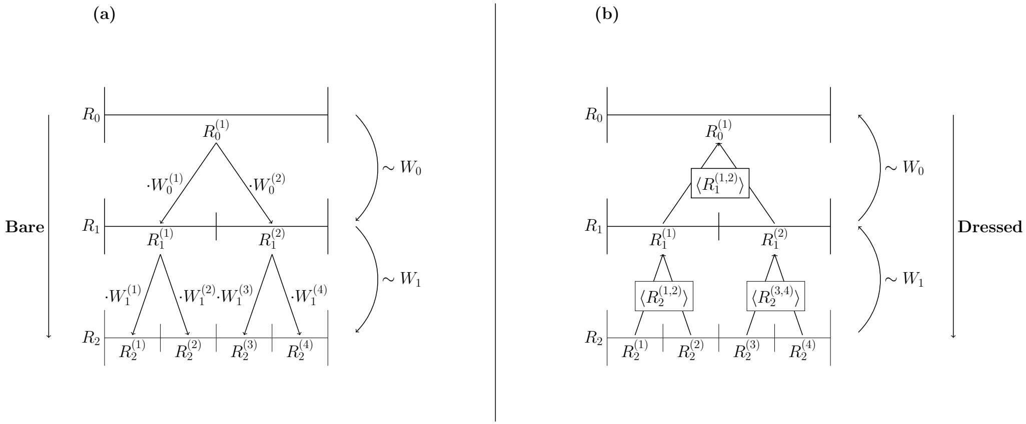

Fig. 1. A basic rainfall model, graphically illustrated. The left hand side of the image is the dressing procedure, whereas the right hand side is the generation.

HESSD
10, 11385–11422, 2013

Imperfect scaling in rainfall

van den Berg et al.

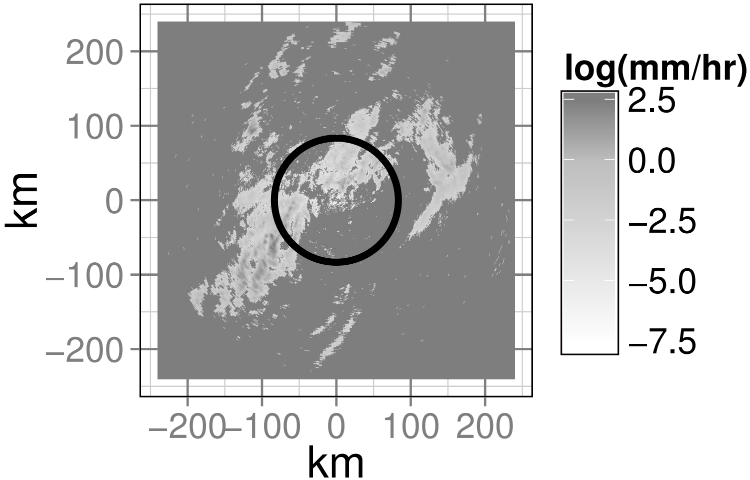

Fig. 2. A log-transformed rainfall field, together with the radius of reliable observations.

HESSD
10, 11385–11422, 2013

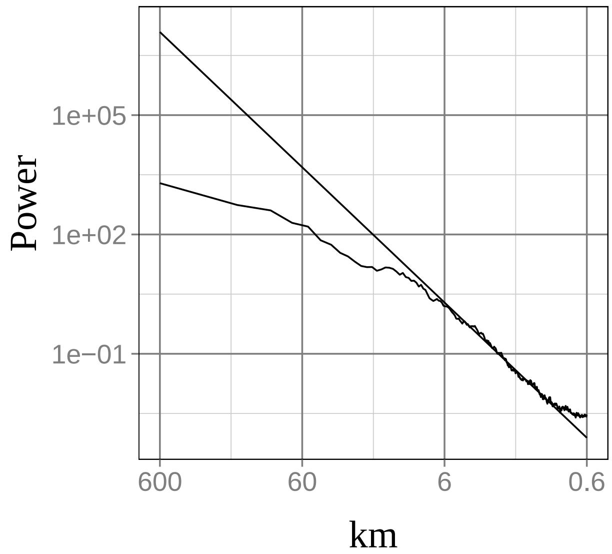

Fig. 3. The power spectrum of the field of storm 1 at time 1.

HESSD
10, 11385–11422, 2013

Imperfect scaling in rainfall

van den Berg et al.

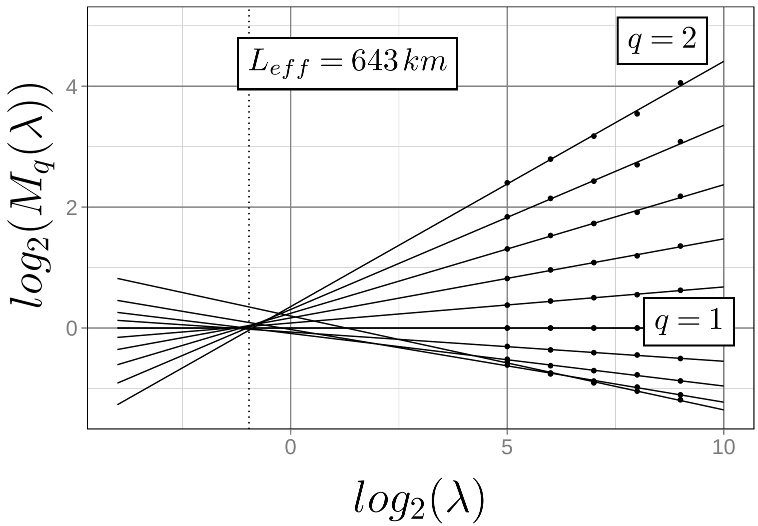

Fig. 4. The empirical moments M_q as a function of scale.

HESSD
10, 11385–11422, 2013

Imperfect scaling in rainfall

van den Berg et al.

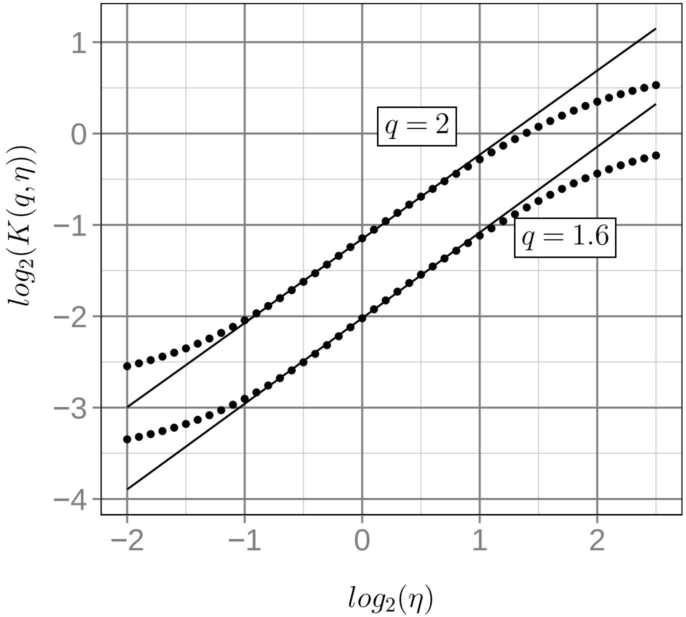

Fig. 5. The double trace moments of the field of storm 1 at time 1.

Discussion Paper | Discussion Paper | Discussion Paper | Discussion Paper |

HESSD

10, 11385–11422, 2013

Imperfect scaling in rainfall

van den Berg et al.

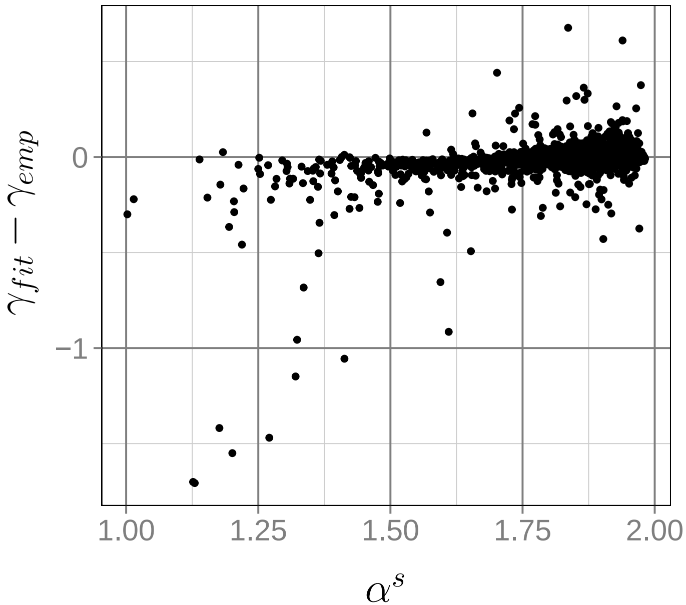

Fig. 6. The difference between the parameter γ at the second coarsest scale, fitted and empirically fitted.

HESSD
10, 11385–11422, 2013

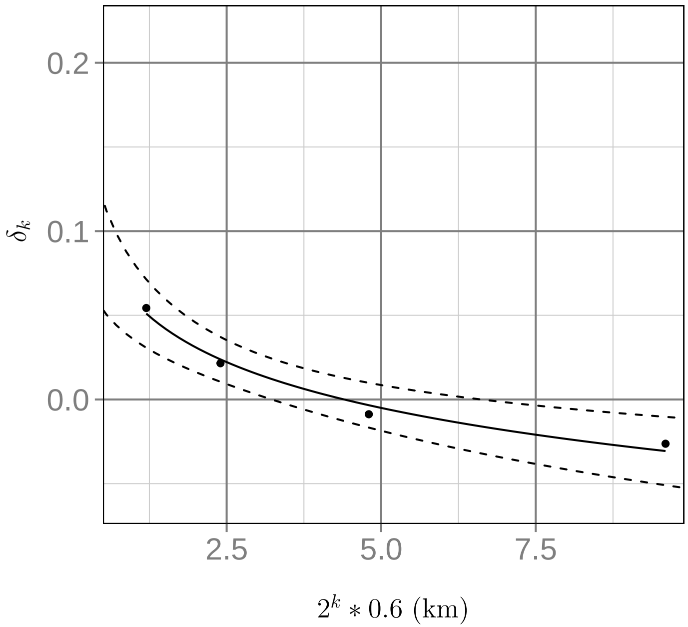

Fig. 7. The empirical means of the increments, averaged over all images, and its fit.

HESSD
10, 11385–11422, 2013

Imperfect scaling in rainfall

van den Berg et al.

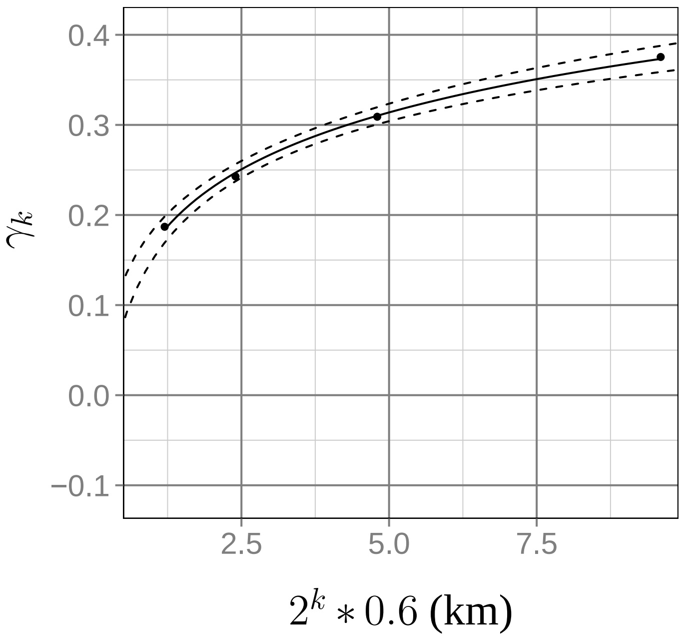

Fig. 8. The empirically fitted γ of the increments, averaged over all images, and its fit.

Discussion Paper | Discussion Paper | Discussion Paper | Discussion Paper |

HESSD

10, 11385–11422, 2013

Imperfect scaling in rainfall

van den Berg et al.

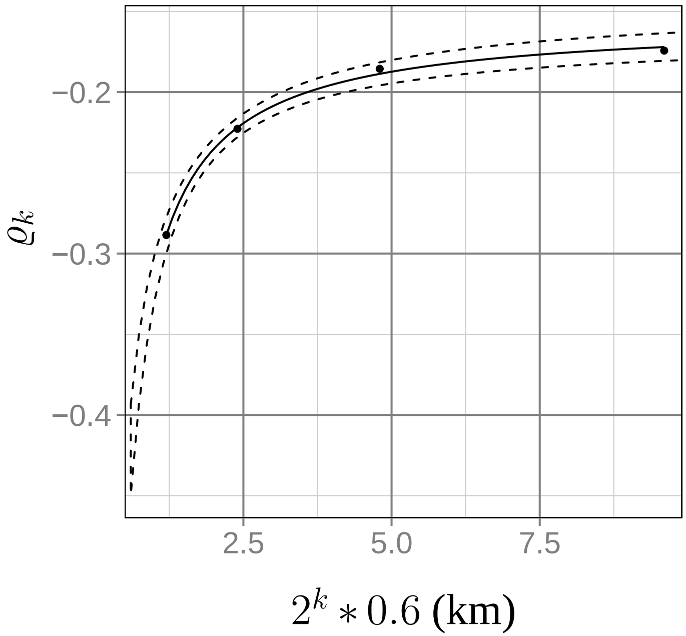

Fig. 9. The empirical ϱ of the increments, averaged over all images, and its fit.

HESSD
10, 11385–11422, 2013

Imperfect scaling in rainfall

van den Berg et al.

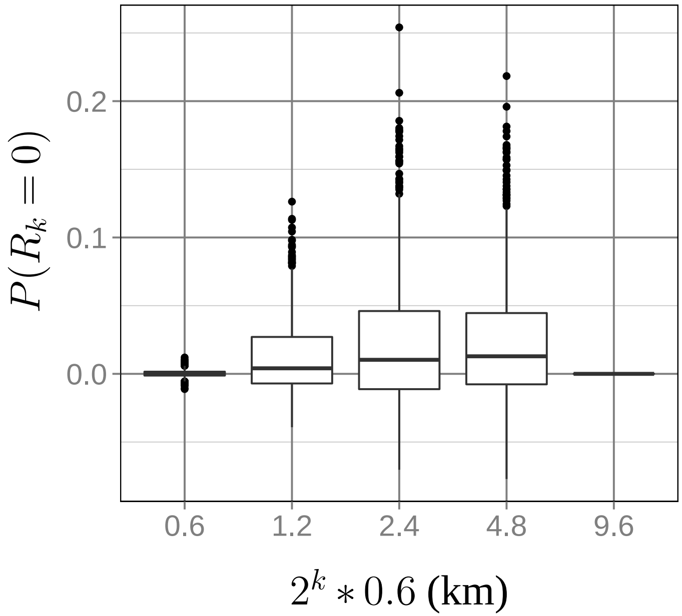

Fig. 10. The difference between the probability of dry pixels as predicted, and as observed.

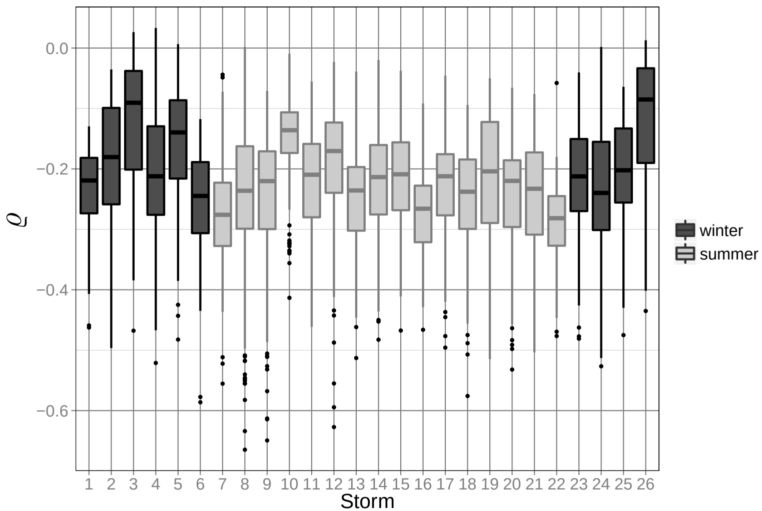

Fig. 11. The correlations of all scales for each of the storms.

HESSD
10, 11385–11422, 2013

Imperfect scaling in rainfall

van den Berg et al.

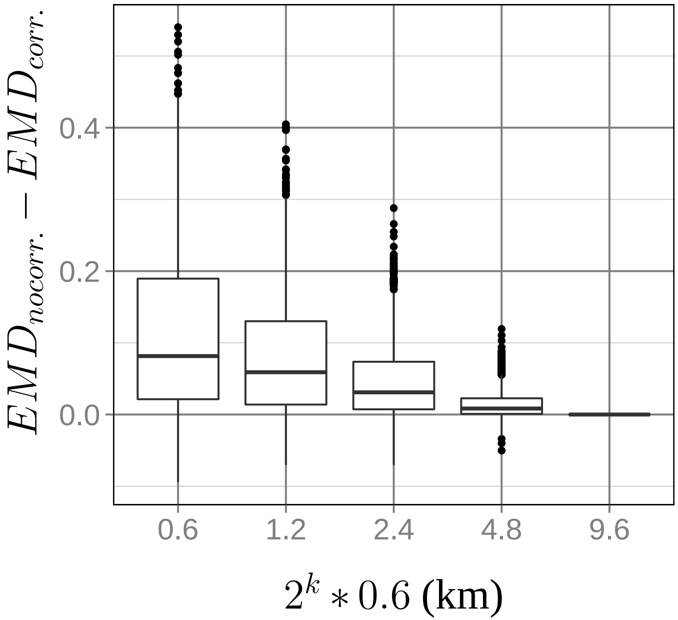

Fig. 12. The difference between the EMD of the distribution without correlation, and that with correlation.

Discussion Paper | Discussion Paper | Discussion Paper | Discussion Paper |

HESSD

10, 11385–11422, 2013

Imperfect scaling in rainfall

van den Berg et al.

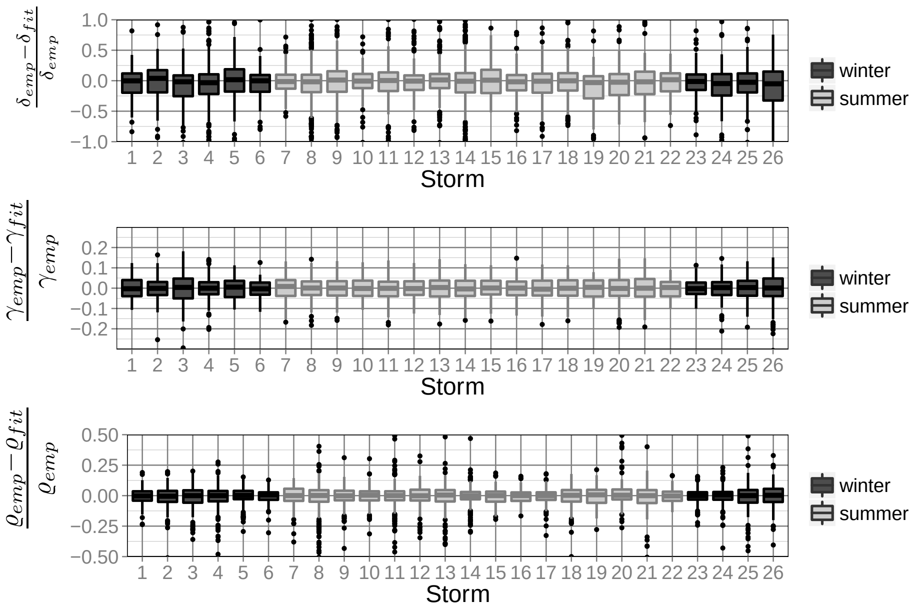

Fig. 13. The relative errors of the mean, shape and correlation parameters.

HESSD

10, 11385–11422, 2013

Imperfect scaling in rainfall

van den Berg et al.

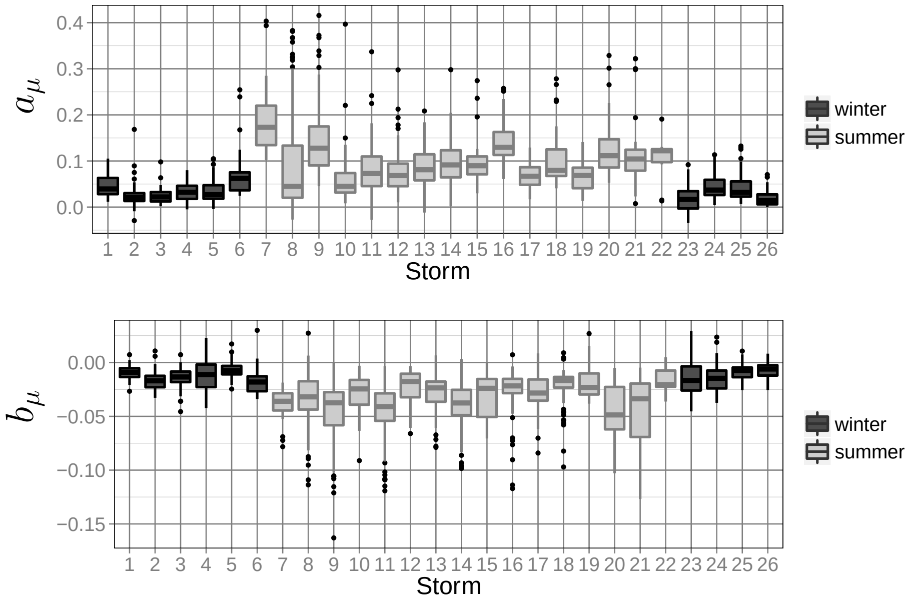

Fig. 14. The parameters for the mean of the increment, shown as boxplots for each storm.

HESSD
10, 11385–11422, 2013

Imperfect scaling in rainfall

van den Berg et al.

Title Page
Abstract | Introduction
Conclusions | References
Tables | Figures
◀| |▶
◀ ▶
Back | Close
Full Screen / Esc
Printer-friendly Version
Interactive Discussion

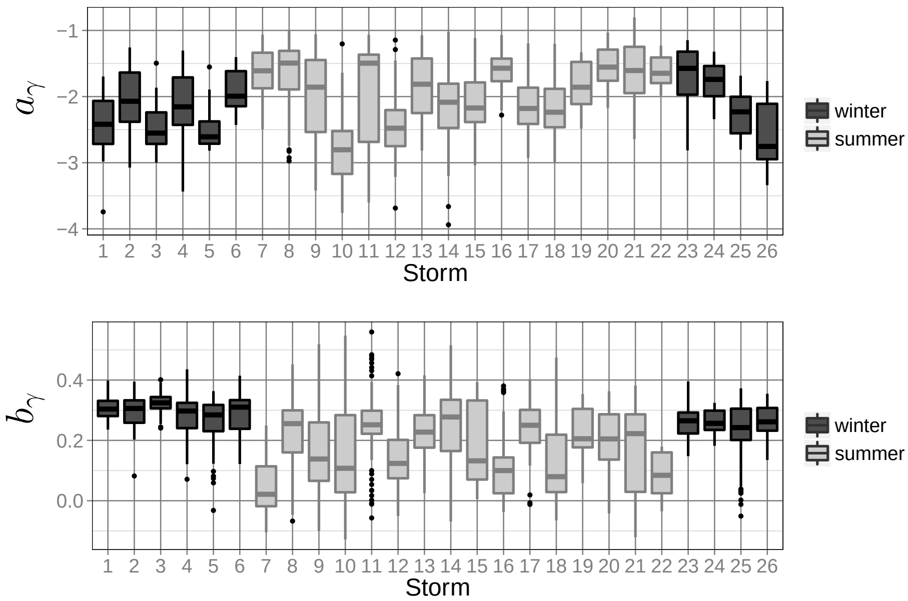

Fig. 15. The parameters for the γ of the increment, shown as boxplots for each storm.

HESSD
10, 11385–11422, 2013

Imperfect scaling in rainfall

van den Berg et al.

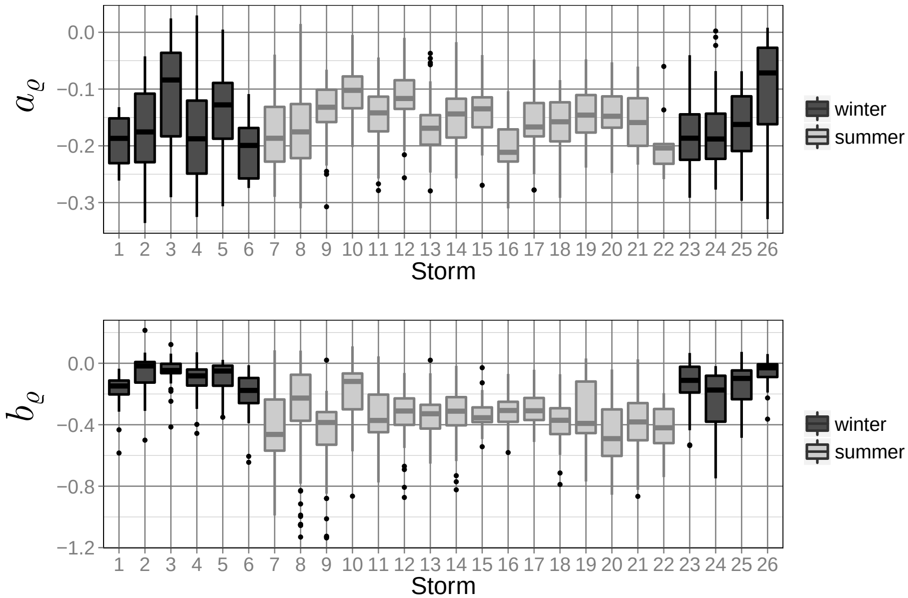

Fig. 16. The parameters for the correlation of the increment, shown as boxplots for each storm.

HESSD
10, 11385–11422, 2013

Imperfect scaling in rainfall

van den Berg et al.

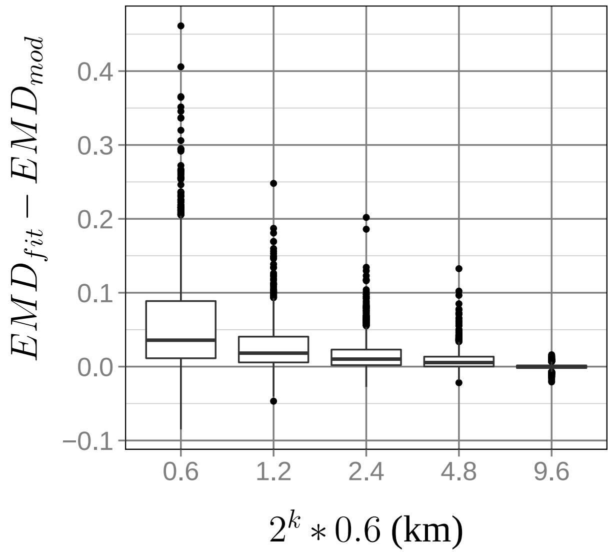

Fig. 17. The difference between the EMD of the direct fit and the EMD of the modelled distribution.

HESSD
10, 11385–11422, 2013